Available online at www.sciencedirect.com
SCIENCE DIRECT
Journal of Molecular Structure 795 (2006) 219–229
Journal of MOLECULAR STRUCTURE
www.elsevier.com/locate/molstruc

Rotational spectroscopy of S_2O: Vibrational satellites, ^{33}S isotopomers, and the sub-millimeter-wave spectrum

S. Thorwirth [a,b,*], P. Theulé [a,b,1], C.A. Gottlieb [a,b], H.S.P. Müller [c], M.C. McCarthy [a,b], P. Thaddeus [a,b]

[a] Division of Engineering and Applied Sciences, Harvard University, Cambridge, MA 02138, USA
[b] Harvard-Smithsonian Center for Astrophysics, Cambridge, MA 02138, USA
[c] I. Physikalisches Institut, Universität zu Köln, Zülpicher Strasse 77, 50937 Köln, Germany

Received 20 January 2006; received in revised form 21 February 2006; accepted 22 February 2006
Available online 2 June 2006

This work is dedicated to Prof. Dr. Gisbert Winnewisser on the occasion of his 70th birthday, in recognition of his many contributions to laboratory astrophysics and radio astronomy

Abstract

The rotational spectra of disulfur monoxide, S_2O, and several of its rare isotopic species have been studied in a supersonic molecular beam by Fourier transform microwave spectroscopy. The strongest lines of S_2O were observed by mixing molecular oxygen with sulfur vapor from a heated reservoir at 190 °C, and were so intense that both ^{33}SSO and $S^{33}SO$ were detected in natural abundance, as well as new rotational transitions of ^{34}SSO and $S^{34}SO$. Vibrationally excited states (v_1,v_2,v_3) up to (0,8,0), combination states (0,v_2,1) up to (0,4,1), and the (1,0,0) and (0,0,1) states were also observed in a discharge of SO_2 in neon. In addition, the sub-millimeter-wave spectrum of $^{32}S_2O$ has been studied up to 470 GHz in a free space absorption cell through a discharge of sulfur vapor and SO_2. An extensive set of molecular parameters for the main isotopic species has been obtained by analyzing all of the presently available rotational and rotation–vibration data.

Detection of several new transitions of the SO dimer S_2O_2 at centimeter wavelengths has yielded an improved set of molecular parameters for its ground vibrational state.

Keywords: Sulfur oxides; Disulfur monoxide; S_2O; S_2O_2; Rotational spectroscopy; Hyperfine structure; Vibrational satellites

1. Introduction

Disulfur monoxide, S_2O, was first studied spectroscopically in 1959 by Meschi and Myers in the microwave band [1] in a discharge through sulfur vapor and SO_2. Rotational transitions were detected not only in the ground vibrational state but also in $v_2=1$. Since then, additional investigations have been carried out at higher frequencies [2,3] and the ^{34}S isotopomers have been detected [3]. A microwave study of $S_2^{18}O$ $v_2=0,1$ has also been reported [4] as well as diode laser investigations of the ν_1 (S–O stretching) and ν_3 (S–S stretching) vibrational bands of $S_2^{18}O$ and the main isotopic species, yielding a purely experimental equilibrium structure [5,6]. Highly vibrationally excited S_2O has been seen in laser-induced fluorescence and cavity ring-down experiments (see, e.g. Ref. [7]). A summary of the spectroscopic investigations of S_2O is given by Steudel [8].

In recent radio studies of S_3 and S_4 in this laboratory [9–11], fairly strong lines of S_2O were observed as an impurity, prompting us to undertake a new study of this molecule, deliberately adding molecular oxygen or sulfur dioxide to the source to produce even stronger lines. This new study, which greatly extends the previous work, includes: (i) a Fourier transform microwave (FTM) investigation of rotational transitions of S_2O in the ground vibrational state as well as vibrational satellites from (v_1,v_2,v_3)=(1,0,0), (0,0,1), (0,v_2,0) up to $v_2=8$, and the combination modes (0,v_2,1) up to $v_2=4$; (ii) an FTM investigation of the mono ^{34}S and ^{33}S isotopic species; and (iii) a millimeter and sub-millimeter wave investigation of

* Corresponding author. Present address: Max-Planck-Institut für Radioastronomie, Auf dem Hügel 69, 53121 Bonn, Germany.
E-mail address: sthorwirth@mpifr-bonn.mpg.de (S. Thorwirth).
[1] Present address: Physique des interactions ioniques et moléculaires, Centre de Saint Jérôme, Université de Provence, 13397 Marseille Cedex 20, France.

0022-2860/$ - see front matter © 2006 Elsevier B.V. All rights reserved.
doi:10.1016/j.molstruc.2006.02.055

S_2O in the ground vibrational state to frequencies as high as 470 GHz.

2. Experimental

The FTM spectrometer used in the present investigation, described in detail elsewhere [12,13], operates between 5 and 42 GHz. Transient molecules are produced in the throat of a pulsed nozzle through a stream of appropriate precursor gases heavily diluted in a buffer gas (typically Ne or Ar). Free expansion from the nozzle into the large vacuum chamber of the spectrometer forms a supersonic beam moving at about twice the speed of sound. As the molecules approach the center of the Fabry–Perot cavity, rotational transitions are excited by a short pulse of resonant microwave radiation. Transient line emission from the coherently rotating molecules is then detected by a sensitive microwave receiver, and the Fourier transform of this decaying signal then yields the desired power spectrum. In the present experimental configuration with the molecular beam oriented along the axis of the Fabry–Perot cavity, each line is split into two well-resolved Doppler components corresponding to the two traveling waves, which compose the standing wave of the Fabry–Perot mode.

With a discharge, fairly strong lines of S_2O are produced from SO_2 (0.2% in neon), but even stronger ones are obtained without a discharge by simply mixing molecular oxygen (0.2% in neon) with sulfur vapor at a temperature of about 190 °C (using the same heated nozzle as in our recent study of S_3 and S_4). This technique was used to study the ground state rotational spectra of S_2O and its mono-^{34}S and ^{33}S isotopic species (the latter for the first time). The real purpose of a discharge in the present work is to vibrationally excite S_2O, and to allow us to measure vibrational satellites in the rotational spectrum (see, e.g. Ref. [14]). Using this method, vibrational satellites of S_2O from a total of 14 vibrational states were observed. Source conditions were a stagnation pressure behind the pulsed valve of 3.5 atm and a discharge potential of 1.0–1.3 kV.

The millimeter-wave study of S_2O was done with the free-space absorption spectrometer in this laboratory [15]. In this instrument, millimeter-wave radiation is generated by a solid-state Gunn oscillator, and then multiplied in frequency to yield useful carrier signals to 500 GHz and beyond. In the present work, experimental parameters were very similar to those adopted for our recent investigation of S_3 and S_4 [11], except that a dilute mixture of SO_2 in argon was used instead of pure argon to increase the amount of oxygen.

The rare isotopic species of S_2O were studied in natural abundance, nearly all only with the FTM spectrometer because of its superior sensitivity.

3. Analysis

Like isovalent SO_2 and S_3, S_2O is bent, with the structural equilibrium parameters $d_{SS} = 188.4$ pm, $d_{SO} = 145.6$ pm and $\alpha_{SSO} = 117.88°$ [6]. Owing to the lower symmetry (C_S instead of C_{2v}), S_2O exhibits both *a*- and *b*-type transitions. The two dipole moment components $\mu_a = 0.875(10)$ D and $\mu_b = 1.18(2)$ D [1] are comparably strong, leading to a fairly dense rotational spectrum dominated by strong *b*-type *Q*-branch and *a*- and *b*-type *R*-branch progressions.

In the least-squares analyses, Pickett's program SPFIT [16] with Watson's Hamiltonian in the *A*-reduction was used throughout. In all tables, 1σ uncertainties (in parentheses) are given in units of the last significant digits.

3.1. The main species, $^{32}S_2O$

Very strong lines of S_2O in the ground and (0,1,0) bending vibrational state were observed with the FTM spectrometer in a discharge through SO_2 in neon. A survey scan around the fundamental *a*-type transition $1_{0,1}$–$0_{0,0}$ at 9566 MHz revealed more than 10 satellites from vibrational states whose pure rotational spectra had not previously been observed (Fig. 1). Rotational transitions from the first excited stretching modes (1,0,0) and (0,0,1) were readily identified on the basis of frequencies calculated with constants determined from a fit to the rotation–vibration data in Lindenmayer et al. [5,6]. In all,

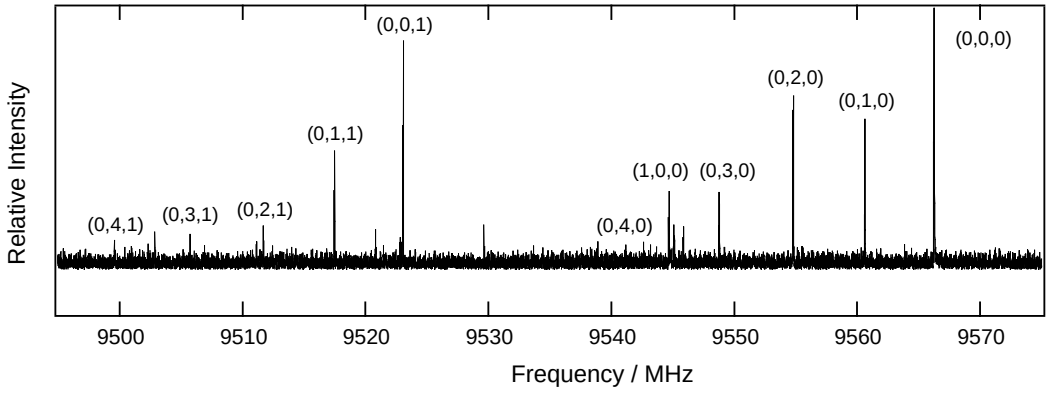

Fig. 1. Vibrational satellite pattern of the $1_{0,1}$–$0_{0,0}$ transition of S_2O. The vibrational states are designated according to (v_1,v_2,v_3). The spectrum is a composite of single spectra recorded with a step size of 400 kHz. Two hundred fifty cycles were averaged at each setting of the Fabry–Perot cavity employing a repetition rate of 6 Hz.

Table 1
Experimental microwave transition frequencies of S_2O in the ground vibrational and first excited vibrational states (MHz) and residuals *o–c* (kHz, global fit)

Transition	(0,0,0)	*o–c*	(1,0,0)	*o–c*	(0,1,0)	*o–c*	(0,0,1)	*o–c*
$2_{1,2}$–$3_{0,3}$	7635.6394(20)	0.3	7331.3709(20)	0.8	8209.2989(20)	0.4	7790.6101(20)	−0.7
$1_{0,1}$–$0_{0,0}$	9566.2535(20)	0.1	9544.6729(20)	−1.1	9560.6089(20)	−0.2	9523.0528(20)	0.3
$5_{0,5}$–$4_{1,4}$	13258.9405(20)	−1.3	13522.6729(20)	1.0	12696.7339(30)	−0.1	13009.9395(20)	−0.6
$1_{1,1}$–$2_{0,2}$	17728.9092(20)	1.3	17404.1709(20)	0.5	18303.6572(20)	0.7	17838.2598(20)	0.3
$2_{1,2}$–$1_{1,1}$	18580.7120(20)	0.8	18536.0606(20)	0.8	18562.4414(20)	−0.5	18496.9815(20)	1.5
$2_{0,2}$–$1_{0,1}$	19126.3106(20)	0.4	19083.0557(20)	−0.2	19114.9600(20)	0.3	19039.9707(20)	−0.6
$2_{1,1}$–$1_{1,0}$	19684.4688(20)	0.2	19642.8037(20)	−0.8	19680.1709(20)	1.0	19595.3956(20)	0.0
$3_{1,3}$–$2_{1,2}$	27867.1533(20)	1.2	27800.1163(20)	0.7	27839.7100(20)	0.1	27741.5938(20)	−0.6
$3_{0,3}$–$2_{0,2}$	28673.9805(20)	0.5	28608.8594(20)	−0.6	28656.7998(20)	−0.1	28544.6299(20)	1.1
$3_{1,2}$–$2_{1,1}$	29522.7061(20)	2.2	29460.1465(20)	−0.1	29516.2178(20)	0.6	29389.1348(20)	0.6
$2_{1,1}$–$2_{0,2}$	37965.2618(20)	−1.6	37600.3555(20)	−0.2	38542.6973(20)	−1.3	37982.8711(20)	−0.1
$4_{0,4}$–$3_{0,3}$	38203.1016(30)	1.4	–		–		–	
$3_{1,2}$–$3_{0,3}$	38813.9883(20)	0.9	–		–		–	

46 lines for the ground and first excited vibrational states (Table 1), and 61 lines from overtones of ν_2 with $2 \leq v_2 \leq 8$ and combinations modes of ν_2 and ν_3 with $v_2 \leq 4$, were measured in the centimeter-wave band (Table 2).

Following the FTM investigation, a millimeter/sub-millimeter wave study of the ground vibrational state was undertaken at frequencies as high as 470 GHz. Prior to this work, rotational lines of S_2O had not been measured above 140 GHz [2]. A total of 139 lines were measured (see Table 3; unresolved asymmetry doublets are counted only once). Sample spectra showing *a*-type *R*-branch transitions that are rather close to oblate pairing are shown in Fig. 2.

Two sets of spectroscopic parameters of $^{32}S_2O$ are given in Table 4. In Fit 1, the constants for the ground state were obtained from the pure rotational data of the (0,0,0) state, the rotation–vibration data of the (1,0,0) and (0,0,1) states and the vibrational satellite data of the latter two states. In Fit 2, all pure rotational and rotation–vibration data presently available were analyzed in a global fit in which each rotational and centrifugal distortion constant X_v in the Hamiltonian has the following general form

$$X_v = X_e + \sum_{i=1}^{3} \alpha_i^X \left(v_i + \frac{1}{2}\right) + \sum_{i,j=1}^{3} \beta_{ij}^X \left(v_i + \frac{1}{2}\right)\left(v_j + \frac{1}{2}\right) + \sum_{i,j,k=1}^{3} \gamma_{ijk}^X \left(v_i + \frac{1}{2}\right)\left(v_j + \frac{1}{2}\right)\left(v_k + \frac{1}{2}\right) + \cdots, \quad (1)$$

where the subscripts *i*, *j*, and *k* refer to the corresponding vibrational modes. Eq. (1) is an extension of the Dunham expressions for a diatomic molecule (see, e.g. Ref. [17]). In

Table 2
Vibrational satellites of S_2O (MHz) and residuals (kHz, global fit)

Transition	(0,2,0)	*o–c*	(0,3,0)	*o–c*	(0,4,0)	*o–c*	(0,5,0)	*o–c*
$1_{0,1}$–$0_{0,0}$	9554.7837(20)	0.3	9548.7769(20)	0.8	9542.5869(20)	0.0	9536.2154(20)	0.1
$2_{1,2}$–$1_{1,1}$	18543.8360(20)	−0.8	18524.9034(20)	2.8	18505.6387(20)	0.3	18486.0557(20)	0.7
$2_{0,2}$–$1_{0,1}$	19103.2500(20)	−0.2	19091.1797(20)	−1.1	19078.7500(20)	−1.1	19065.9610(20)	0.5
$2_{1,1}$–$1_{1,0}$	19675.4814(20)	−0.4	19670.3985(20)	0.4	19664.9131(20)	0.5	19659.0196(20)	0.5
$3_{1,3}$–$2_{1,2}$	27811.7657(20)	−0.3	27783.3272(20)	−0.5	27754.4004(20)	−2.1	27725.0000(30)	2.1
$3_{0,3}$–$2_{0,2}$	28639.0889(20)	−0.8	28620.8477(20)	−1.0	28602.0762(20)	−0.1	28582.7725(20)	1.0
$3_{1,2}$–$2_{1,1}$	–		–		29493.2285(30)	−0.1	29484.3584(20)	−0.2
$4_{1,4}$–$3_{1,3}$	37074.9727(30)	3.2	37036.9883(30)	−0.3	36998.3613(30)	−1.3	36959.1016(30)	0.2
$4_{0,4}$–$3_{0,3}$	38156.0215(20)	1.9	38131.4414(20)	−1.4	–		38080.2149(30)	2.1
Transition	(0,6,0)	*o–c*	(0,7,0)	*o–c*	(0,8,0)	*o–c*	(0,1,1)	*o–c*
$1_{0,1}$–$0_{0,0}$	9529.6607(20)	−0.4	–		9516.0034(20)	−0.1	9517.4732(20)	0.7
$2_{1,2}$–$1_{1,1}$	–		–		–		18478.7461(20)	−0.2
$2_{0,2}$–$1_{0,1}$	19052.8086(20)	0.3	19039.2930(20)	−0.9	19025.4180(20)	1.3	19028.7461(20)	−1.3
$2_{1,1}$–$1_{1,0}$	–		–		–		19591.3193(20)	0.3
$3_{1,3}$–$2_{1,2}$	–		–		–		27714.2022(20)	−1.8
$3_{0,3}$–$2_{0,2}$	28562.9336(20)	−0.1	28542.5606(20)	−1.4	–		28527.6328(20)	−0.1
$3_{1,2}$–$2_{1,1}$	–		–		–		29382.9805(30)	1.3
Transition	(0,2,1)	*o–c*	(0,3,1)	*o–c*	(0,4,1)	*o–c*		
$1_{0,1}$–$0_{0,0}$	9511.7027(20)	−0.6	9505.7456(20)	1.1	9499.5962(20)	0.5		
$2_{1,2}$–$1_{1,1}$	18460.1621(20)	−0.2	18441.2344(20)	1.3	18421.9620(20)	−1.5		
$2_{0,2}$–$1_{0,1}$	19017.1495(20)	1.1	19005.1748(20)	1.0	18992.8213(20)	−1.6		
$2_{1,1}$–$1_{1,0}$	19586.8340(20)	−1.5	19581.9365(30)	−2.2	–			
$3_{0,3}$–$2_{0,2}$	28510.0830(20)	−0.1	28491.9805(20)	1.7	28473.3203(30)	1.2		

Table 3
Experimental millimeter- and sub-millimeter-wave transition frequencies of S_2O in the ground vibrational state and residuals (MHz, global fit)

Transition	Frequency	*o–c*
$32_{2,30}$–$32_{1,31}$	163895.727(20)	0.007
$54_{11,44}$–$55_{10,45}$	245248.439(20)	−0.005
$54_{11,43}$–$55_{10,46}$	245248.439(20)	−0.005
$69_{13,57}$–$70_{12,58}$	246507.467(40)	0.016
$69_{13,56}$–$70_{12,59}$	246507.467(40)	0.016
$26_{10,16}$–$25_{10,15}$	248963.124(20)	0.012
$26_{10,17}$–$25_{10,16}$	248963.124(20)	0.012
$26_{11,15}$–$25_{11,14}$	248965.204(20)	0.007
$26_{11,16}$–$25_{11,15}$	248965.204(20)	0.007
$26_{9,17}$–$25_{9,16}$	248975.397(20)	−0.012
$26_{9,18}$–$25_{9,17}$	248975.397(20)	−0.012
$26_{12,14}$–$25_{12,13}$	248977.922(20)	−0.013
$26_{12,15}$–$25_{12,14}$	248977.922(20)	−0.013
$26_{13,13}$–$25_{13,12}$	248998.980(20)	0.010
$26_{13,14}$–$25_{13,13}$	248998.980(20)	0.010
$26_{8,19}$–$25_{8,18}$	249008.334(20)	0.005
$26_{8,18}$–$25_{8,17}$	249008.334(20)	0.005
$26_{14,12}$–$25_{14,11}$	249026.730(20)	−0.013
$26_{14,13}$–$25_{14,12}$	249026.730(20)	−0.013
$26_{15,11}$–$25_{15,10}$	249060.188(20)	0.011
$26_{15,12}$–$25_{15,11}$	249060.188(20)	0.011
$26_{7,20}$–$25_{7,19}$	249073.052(20)	−0.004
$26_{7,19}$–$25_{7,18}$	249073.052(20)	−0.004
$26_{17,9}$–$25_{17,8}$	249141.141(20)	0.007
$26_{17,10}$–$25_{17,9}$	249141.141(20)	0.007
$26_{18,8}$–$25_{18,7}$	249187.652(20)	0.010
$26_{18,9}$–$25_{18,8}$	249187.652(20)	0.010
$26_{19,7}$–$25_{19,6}$	249237.685(20)	0.011
$26_{19,8}$–$25_{19,7}$	249237.685(20)	0.011
$26_{3,24}$–$25_{3,23}$	249242.588(20)	−0.020
$26_{20,6}$–$25_{20,5}$	249290.949(20)	0.004
$26_{20,7}$–$25_{20,6}$	249290.949(20)	0.004
$26_{21,5}$–$25_{21,4}$	249347.215(20)	0.000
$26_{21,6}$–$25_{21,5}$	249347.215(20)	0.000
$26_{5,22}$–$25_{5,21}$	249403.523(20)	−0.005
$26_{22,4}$–$25_{22,3}$	249406.269(20)	−0.010
$26_{22,5}$–$25_{22,4}$	249406.269(20)	−0.010
$27_{1,27}$–$26_{0,26}$	250252.926(20)	0.000
$38_{9,30}$–$39_{8,31}$	253407.272(20)	−0.037
$38_{9,29}$–$39_{8,32}$	253407.272(20)	−0.037
$53_{11,43}$–$54_{10,44}$	255059.168(20)	−0.013
$53_{11,42}$–$54_{10,45}$	255059.168(20)	−0.013
$7_{5,3}$–$8_{4,4}$	257160.680(20)	0.006
$7_{5,2}$–$8_{4,5}$	257160.680(20)	0.006
$22_{4,19}$–$22_{3,20}$	259190.384(20)	0.005
$45_{10,36}$–$46_{9,37}$	259193.191(20)	0.018
$45_{10,35}$–$46_{9,38}$	259193.191(20)	0.018
$11_{4,7}$–$11_{3,8}$	259415.944(20)	0.001
$13_{4,10}$–$13_{3,11}$	259419.832(20)	−0.009
$11_{4,8}$–$11_{3,9}$	259542.283(20)	−0.013
$9_{4,6}$–$9_{3,7}$	259629.447(20)	−0.025
$25_{4,22}$–$25_{3,23}$	259932.009(20)	−0.014
$26_{4,23}$–$26_{3,24}$	260380.413(20)	−0.009
$60_{12,49}$–$61_{11,50}$	260621.874(20)	−0.005
$60_{12,48}$–$61_{11,51}$	260621.874(20)	−0.005
$27_{4,24}$–$27_{3,25}$	260955.616(20)	0.004
$28_{4,25}$–$28_{3,26}$	261673.852(20)	−0.005
$29_{4,26}$–$29_{3,27}$	262551.498(20)	0.001
$37_{9,29}$–$38_{8,30}$	263166.319(20)	0.015
$37_{9,28}$–$38_{8,31}$	263166.319(20)	0.015
$36_{3,34}$–$36_{2,35}$	263474.829(20)	−0.001
$30_{4,27}$–$30_{3,28}$	263604.730(20)	−0.011
$31_{4,28}$–$31_{3,29}$	264849.472(20)	0.005

Table 3 (*continued*)

Transition	Frequency	*o–c*
$32_{4,29}$–$32_{3,30}$	266301.037(20)	0.015
$42_{12,30}$–$43_{11,33}$	435224.649(30)	−0.007
$42_{12,31}$–$43_{11,32}$	435224.649(30)	−0.007
$47_{1,46}$–$46_{2,45}$	435276.512(30)	−0.005
$41_{3,39}$–$40_{2,38}$	436318.613(30)	−0.031
$48_{0,48}$–$47_{1,47}$	436656.451(30)	−0.018
$48_{1,48}$–$47_{1,47}$	436690.197(30)	0.005
$48_{0,48}$–$47_{0,47}$	436698.000(30)	0.002
$48_{1,48}$–$47_{0,47}$	436731.731(30)	0.009
$34_{11,23}$–$35_{10,26}$	439224.944(30)	0.005
$34_{11,24}$–$35_{10,25}$	439224.944(30)	0.005
$46_{14,32}$–$45_{14,31}$	440432.445(50)	0.021
$46_{14,33}$–$45_{14,32}$	440432.445(50)	0.021
$46_{13,33}$–$45_{13,32}$	440438.270(50)	0.053
$46_{13,34}$–$45_{13,33}$	440438.270(50)	0.053
$46_{15,31}$–$45_{15,30}$	440447.360(50)	−0.005
$46_{15,32}$–$45_{15,31}$	440447.360(50)	−0.005
$46_{16,30}$–$45_{16,29}$	440479.039(30)	0.000
$46_{16,31}$–$45_{16,30}$	440479.039(30)	0.000
$46_{17,29}$–$45_{17,28}$	440524.569(30)	0.011
$46_{17,30}$–$45_{17,29}$	440524.569(30)	0.011
$46_{11,35}$–$45_{11,34}$	440537.645(30)	0.003
$46_{11,36}$–$45_{11,35}$	440537.645(30)	0.003
$46_{18,28}$–$45_{18,27}$	440581.778(30)	−0.007
$46_{18,29}$–$45_{18,28}$	440581.778(30)	−0.007
$46_{10,37}$–$45_{10,36}$	440652.798(30)	−0.001
$46_{10,36}$–$45_{10,35}$	440652.798(30)	−0.001
$42_{3,40}$–$41_{2,39}$	440744.975(30)	−0.011
$46_{9,38}$–$45_{9,37}$	440837.070(30)	−0.019
$46_{9,37}$–$45_{9,36}$	440837.070(30)	−0.019
$46_{7,40}$–$45_{7,39}$	441583.748(30)	0.024
$46_{7,39}$–$45_{7,38}$	441600.318(30)	−0.007
$46_{6,41}$–$45_{6,40}$	442259.387(30)	0.001
$46_{6,40}$–$45_{6,39}$	442510.077(30)	−0.003
$46_{5,42}$–$45_{5,41}$	442756.927(30)	−0.003
$58_{3,56}$–$58_{2,57}$	443223.450(30)	0.011
$48_{1,47}$–$47_{2,46}$	444512.230(30)	0.001
$46_{5,41}$–$45_{5,40}$	445050.663(30)	−0.001
$24_{3,21}$–$23_{2,22}$	445225.357(30)	−0.007
$43_{3,41}$–$42_{2,40}$	445469.289(20)	−0.004
$53_{3,50}$–$52_{4,49}$	445528.790(30)	−0.002
$49_{0,49}$–$48_{1,48}$	445642.747(30)	−0.002
$49_{1,49}$–$48_{1,48}$	445670.117(30)	−0.000
$49_{0,49}$–$48_{0,48}$	445676.473(30)	0.001
$49_{1,49}$–$48_{0,48}$	445703.833(30)	−0.008
$56_{14,42}$–$57_{13,45}$	445876.513(30)	−0.030
$56_{14,43}$–$57_{13,44}$	445876.513(30)	−0.030
$69_{5,65}$–$69_{4,66}$	446143.328(30)	0.012
$18_{9,9}$ − $19_{8,12}$	446475.954(30)	0.004
$18_{9,10}$–$19_{8,11}$	446475.954(30)	0.004
$48_{2,47}$–$47_{1,46}$	447206.382(30)	0.018
$20_{4,17}$–$19_{3,16}$	447820.218(30)	−0.027
$33_{11,22}$–$34_{10,25}$	448834.908(30)	0.005
$33_{11,23}$–$34_{10,24}$	448834.908(30)	0.005
$44_{3,42}$–$43_{2,41}$	450503.258(30)	0.068
$59_{3,57}$–$59_{2,58}$	452290.555(30)	−0.005
$54_{1,53}$–$54_{0,54}$	452394.733(30)	−0.002
$25_{10,15}$–$26_{9,18}$	452578.667(30)	0.000
$25_{10,16}$–$26_{9,17}$	452578.667(30)	0.000
$70_{5,66}$–$70_{4,67}$	453998.820(30)	0.040
$50_{0,50}$–$49_{1,49}$	454626.326(30)	0.002
$50_{1,50}$–$49_{1,49}$	454648.520(30)	−0.002
$50_{0,50}$–$49_{0,49}$	454653.680(30)	−0.012
$66_{3,63}$–$66_{2,64}$	455409.466(30)	0.006
$55_{14,41}$–$56_{13,44}$	455493.311(50)	0.087

Table 3 (*continued*)

Transition	Frequency	*o–c*
$55_{14,42}$–$56_{13,43}$	455493.311(50)	0.087
$17_{9,8}$–$18_{8,11}$	456057.253(30)	0.007
$17_{9,9}$–$18_{8,10}$	456057.253(30)	0.007
$65_{4,62}$–$65_{3,63}$	457306.946(30)	−0.048
$13_{5,9}$–$12_{4,8}$	458102.134(30)	−0.006
$13_{5,8}$–$12_{4,9}$	458105.336(30)	−0.035
$55_{7,48}$–$55_{6,49}$	458436.121(30)	0.011
$32_{11,21}$–$33_{10,24}$	458439.595(30)	0.012
$32_{11,22}$–$33_{10,23}$	458439.595(30)	0.012
$60_{2,58}$–$60_{1,59}$	458894.946(30)	0.025
$66_{7,60}$–$66_{6,61}$	459783.673(30)	−0.015
$67_{7,61}$–$67_{6,62}$	459854.330(30)	−0.001
$65_{7,59}$–$65_{6,60}$	459869.325(30)	0.045
$25_{3,22}$–$24_{2,23}$	460473.047(30)	−0.004
$69_{7,63}$–$69_{6,64}$	460527.746(30)	−0.009
$21_{4,17}$–$20_{3,18}$	460775.735(30)	0.028
$54_{3,51}$–$53_{4,50}$	460845.741(30)	−0.006
$62_{7,56}$–$62_{6,57}$	460905.331(30)	−0.015
$48_{7,42}$–$47_{7,41}$	460907.816(30)	−0.025
$48_{7,41}$–$47_{7,40}$	460936.258(30)	0.014
$60_{3,58}$–$60_{2,59}$	461375.540(30)	0.002
$61_{7,55}$–$61_{6,56}$	461459.107(30)	−0.000
$55_{1,54}$–$55_{0,55}$	461541.835(30)	−0.005
$55_{2,54}$–$55_{1,55}$	461869.046(30)	−0.004
$71_{7,65}$–$71_{6,66}$	462013.775(30)	−0.017
$71_{5,67}$–$71_{4,68}$	462023.503(30)	−0.028
$48_{5,44}$–$47_{5,43}$	462036.559(30)	−0.007
$48_{6,42}$–$47_{6,41}$	462036.559(30)	−0.007
$24_{10,14}$–$25_{9,17}$	462170.058(30)	0.030
$24_{10,15}$ − $25_{9,16}$	462170.058(30)	0.030
$59_{7,53}$–$59_{6,54}$	462791.921(30)	0.010
$50_{1,49}$–$49_{2,48}$	462862.236(30)	−0.017
$58_{7,52}$–$58_{6,53}$	463544.207(30)	0.011
$51_{0,51}$–$50_{1,50}$	463607.388(30)	−0.016
$51_{1,51}$–$50_{1,50}$	463625.391(30)	−0.008
$51_{0,51}$–$50_{0,50}$	463629.596(30)	−0.006
$51_{1,51}$–$50_{0,50}$	463647.618(30)	0.021
$57_{7,51}$–$57_{6,52}$	464337.278(30)	0.015
$73_{7,67}$–$73_{6,68}$	464428.885(30)	0.018
$6_{6,0}$–$5_{5,1}$	465075.004(30)	−0.006
$6_{6,1}$–$5_{5,0}$	465075.004(30)	−0.006
$56_{7,50}$–$56_{6,51}$	465159.858(30)	−0.021
$16_{9,7}$–$17_{8,10}$	465635.514(30)	0.016
$16_{9,8}$–$17_{8,9}$	465635.514(30)	0.016
$55_{7,49}$–$55_{6,50}$	466001.762(30)	0.002
$74_{7,68}$–$74_{6,69}$	466017.807(30)	−0.011
$51_{7,44}$–$51_{6,45}$	466036.076(30)	−0.013
$54_{7,48}$–$54_{6,49}$	466853.576(30)	−0.021
$50_{7,43}$–$50_{6,44}$	467509.871(30)	0.009
$31_{11,20}$–$32_{10,23}$	468039.336(30)	−0.012
$31_{11,21}$–$32_{10,22}$	468039.336(30)	−0.012
$52_{7,46}$–$52_{6,47}$	468554.783(30)	−0.011
$49_{7,42}$–$49_{6,43}$	468845.854(30)	−0.003
$51_{7,45}$–$51_{6,46}$	469390.399(30)	0.013
$76_{7,70}$–$76_{6,71}$	470015.640(200)	−0.040
$49_{8,42}$–$48_{8,41}$	470017.797(100)	0.029
$49_{8,41}$–$48_{8,40}$	470019.692(100)	−0.012

this case, one also finds the following alternative expressions besides Dunham's formulation:

$$B_v = B_e - \alpha_e\left(v+\frac{1}{2}\right) + \gamma_e\left(v+\frac{1}{2}\right)^2 + \cdots \quad (2)$$

$$D_v = D_e + \beta_e\left(v+\frac{1}{2}\right) + \delta_e\left(v+\frac{1}{2}\right)^2 + \cdots \quad (3)$$

These expressions do not accommodate vibrational corrections to sextic or higher-order centrifugal distortion parameters, so for an asymmetric rotor such as S_2O a more general formulation as given in Eq. (1) is useful. The parameters in Eqs. (2) and (3) are related to the ones in Eq. (1), e.g. $-\alpha_e$ in Eq. (2) corresponds to α^B in Eq. (1). More specifically, each $-\alpha_e$ and β_e in Eqs. (2) and (3) has a corresponding α_i^X in Eq. (1) and each γ_e and δ_e in Eqs. (2) and (3) has a corresponding β_{ij}^X in Eq. (1), and so on.

The new set of spectroscopic constants for $^{32}S_2O$ are given in Table 4. The largest number of vibrational corrections was needed for the ν_2 mode, because lines were measured in states with up to eight quanta. The terms $\gamma_{223}^{B,C}$ were necessary in the treatment of the combination modes $(0,\nu_2,1)$, but only the α_1^X terms were required in the analysis of the S–O stretching mode ν_1 because only the first excited state was observed. In the global analysis (Fit 2), the vibrational dependence is largest for the rotational constants A, B, and C. Generally, differences for $\alpha_v^{A,B,C}$ in Table 4 and $-\alpha_v^{A,B,C}$ in Ref. [6] are quite small (<200 kHz), except for α_2^A which differs by about 18 MHz owing to inclusion of β_{22}^A in the present work. For the quartic centrifugal distortion constants three, four, and four rotation–vibration interaction constants α_i^X could be determined for the ν_1, ν_2, and ν_3 modes, respectively, since the differences between the ground state spectroscopic constants (Fit 1) and the corresponding near-equilibrium constants (Fit 2) are well determined.

In the case of high-order constants virtually no vibrational dependence can be determined from the present data, so X_0 and X_e are nearly the same.

3.2. ^{34}SSO and $S^{34}SO$

The two singly substituted ^{34}S isotopic species were readily observed in the FTM spectrometer near frequencies predicted from the data reported by Tiemann et al. [3]. As summarized in Table 5, 15 lines of ^{34}SSO and 14 of $S^{34}SO$ were measured in the microwave range up to 39 GHz. The most intense lines were recorded in a discharge of SO_2 in neon. Lines which were weak in the discharge source were then measured in the hot sulfur/molecular oxygen source. We did not attempt to detect vibrational satellites of the ^{34}S isotopomers in our discharge source, but that could almost certainly be done. Transition frequencies for both isotopomers were calculated with the new set of spectroscopic constants, and another 24 lines of ^{34}SSO and 27 lines of $S^{34}SO$ were measured in the 90 GHz region, most of which are either *b*-type $^rQ_1$ or *a*-type ($J=10$–9) *R*-branch transitions (Table 6). A combined fit of the data in Ref. [3] and the new data (Tables 5 and 6) yields improved sets of spectroscopic constants (Table 7): all five quartic centrifugal distortion constants and one sextic constant (Φ_{KJ}) have now been determined for both isotopomers. Additional sextic and octic centrifugal distortion constants were taken from $^{32}S_2O$ (Table 4, Fit 1) and kept fixed.

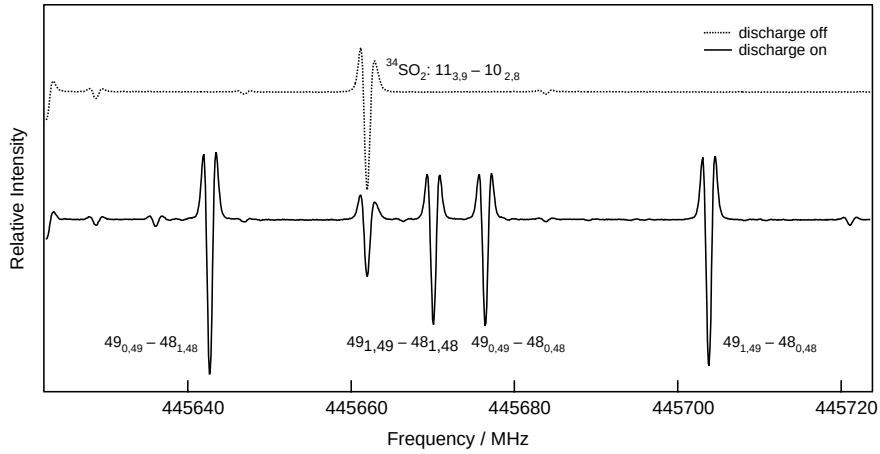

Fig. 2. Sub-millimeter-wave rotational spectrum of S_2O at 446 GHz. The upper (dotted) spectrum was obtained under experimental conditions with the discharge turned off while the lower spectrum demonstrates the presence of S_2O by four $J=49$–48 transitions with the discharge on.

3.3. ^{33}SSO and $S^{33}SO$

The intensity of the S_2O lines in the hot sulfur/oxygen source was sufficiently high to undertake a search for the $1_{0,1}$–$0_{0,0}$ transitions of the two singly substituted ^{33}S isotopomers in natural abundance (0.75%). Initially, the search was based on scaled rotational constants obtained by comparing the equilibrium and ground state rotational constants of the main isotopic species and multiplying these correction factors with the equilibrium rotational constants of ^{33}SSO and $S^{33}SO$. A somewhat more sophisticated estimate can be obtained from rotational parameters evaluated from an S_2O $r_{I,\varepsilon}$ structure [18]. Here, it is assumed that vibrational contributions ε_i to the ground state moments of inertia $I_{0,i}$ are the same for each isotopic species. The interesting aspect of this structural model is that it predicts ground state rotational constants of new isotopic species rather well because of the explicit determination of ε_i (for example see Ref. [19]). Employing data for $^{32}S_2O$, ^{34}SSO, $S^{34}SO$ (this study) and $S_2^{18}O$ [4,6], first estimates of the B_i were determined for ^{33}SSO and $S^{33}SO$. The structural fit had residuals for B and C of less than 100 kHz while those of the much larger A constant were less than 750 kHz. The best estimates of the rotational parameters of the ^{33}S isotopic species were obtained by correcting the initial estimates on the assumption that the residuals of ^{33}SSO and $S^{33}SO$ in a structural fit lie between those of S_2O and the corresponding ^{34}S isotopic species (Table 9). Effects of centrifugal distortion on the low-J transitions are small, nevertheless to further improve our estimates for rotational transitions of the ^{33}S isotopic species, we assumed that the quartic distortion constants are the mean of the normal and ^{34}S isotopic species. In addition, ^{33}S nuclear quadrupole coupling constants were calculated at the B3LYP/cc-pCVTZ level of theory (GAUSSIAN 03 [20], Table 9).

Guided by these estimates of the transition frequencies the two sulfur-33 isotopic species were detected in the supersonic beam. The spectra shown in Fig. 3 are aligned on the strong central ($F=2.5$–1.5) hyperfine component to illustrate the differences in the hyperfine structure (hfs) of the two isotopic

Table 4
Molecular parameters of S_2O (MHz)

Parameter	Value
Fit 1[a]	
A_0	41915.42761(86)
B_0	5059.09997(13)
C_0	4507.16100(16)
$\Delta_{J0}\times10^3$	1.891474(81)
$\Delta_{JK0}\times10^3$	−32.1264(18)
Δ_{K0}	1.200100(26)
$\delta_{J0}\times10^3$	0.345616(64)
$\delta_{K0}\times10^3$	12.3046(66)
$\Phi_{J0}\times10^9$	1.036(19)
$\Phi_{JK0}\times10^9$	47.0(16)
$\Phi_{KJ0}\times10^6$	−4.874 (11)
$\phi_{K0}\times10^3$	0.12239(25)
$\phi_{J0}\times10^9$	0.568(25)
$\phi_{JK0}\times10^9$	18.4(24)
$\phi_{K0}\times10^6$	5.31(12)
$L_{JJK0}\times10^{12}$	−0.38(11)
$L_{JK0}\times10^{12}$	−5.5(16)
$L_{KKJ0}\times10^9$	0.687(15)
$L_{K0}\times10^9$	−16.36(66)
$l_{J0}\times10^{15}$	−6.7(29)
Fit 2[b]	
A_e	41829.107(91)
B_e	5075.23382(63)
C_e	4526.18911(71)
$\Delta_{Je}\times10^3$	1.8804(12)
$\Delta\ J_{Ke}\times10^3$	−31.308(26)
Δ_{Ke}	1.15927(78)
$\delta_{Je}\times10^3$	0.34371(38)
$\delta_{Ke}\times10^3$	10.94(15)
$\Phi_{Je}\times10^9$	1.036(19)
$\Phi\ J_{Ke}\times10^9$	47.0(16)
$\Phi\ K_{Je}\times10^6$	−4.874(11)
$\phi_{Ke}\times10^3$	0.12241(25)
$\phi_{Je}\times10^9$	0.566(25)
$\phi_{JKe}\times10^9$	18.4(24)
$\phi_{Ke}\times10^6$	5.31(12)
$L_{JJKe}\times10^{12}$	−0.38(11)
$L_{JKe}\times10^{12}$	−5.5(16)
$L_{KKJe}\times10^9$	0.687(15)
$L_{Ke}\times10^9$	−16.41(66)
$l_{Je}\times10^{15}$	−6.5(29)
α_1^A	−378.0507(16)

Table 4 (*continued*)

Parameter	Value
α_1^B	−10.04276(25)
α_1^C	−11.53660(36)
$\alpha_1^{\Delta_J} \times 10^6$	15.14(50)
$\alpha_1^{\Delta_K} \times 10^3$	−15.32(28)
$\alpha_1^{\delta_J} \times 10^6$	4.54(47)
E_1	34969400.6(20)
α_2^A	546.08(24)
α_2^B	0.7354(11)
α_2^C	−6.2348(11)
β_{22}^A	9.04(12)
$\beta_{22}^B \times 10^3$	−48.61(37)
$\beta_{22}^C \times 10^3$	−39.82(36)
$\gamma_{222}^B \times 10^3$	−0.490(38)
$\gamma_{222}^C \times 10^3$	0.436(38)
$\beta_{23}^B \times 10^3$	83.63(88)
$\beta_{23}^C \times 10^3$	−11.27(80)
$\gamma_{223}^B \times 10^3$	−2.40(22)
$\gamma_{223}^C \times 10^3$	−1.58(18)
$\alpha_2^{\Delta_J} \times 10^6$	6.1(22)
$\alpha_2^{\Delta_{JK}} \times 10^3$	−1.202(43)
$\alpha_2^{\Delta_K} \times 10^3$	80.7(15)
$\alpha_2^{\delta_K} \times 10^3$	2.73(30)
$\beta_{22}^{\Delta_K} \times 10^3$	8.0[c]
α_3^A	0.0892(16)
α_3^B	−22.97714(53)
α_3^C	−20.25897(61)
$\alpha_3^{\Delta_J} \times 10^6$	0.87(58)
$\alpha_3^{\Delta_{JK}} \times 10^3$	−0.435(30)
$\alpha_3^{\Delta_K} \times 10^3$	12.32(12)
$\alpha_3^{\delta_J} \times 10^6$	−0.74(59)
E_3	20359987.6(30)

[a] Fit to the rotational and rotation–vibration data of the (0,0,0), (1,0,0), and (0,0,1) states (see Section 3.1).

[b] Global fit to all available rotational and rotation–vibration data (see Section 3.1).

[c] Constrained. Based on the ratios $A_e/\alpha_2^A \approx 75$, $\alpha_2^A/\beta_{22}^A \approx 60$, and $\Delta_{Ke}/\alpha_2^{\Delta_K} \approx 14$ it was assumed that $\alpha_2^{\Delta_K}/\beta_{22}^{\Delta_K}$ is of order 10.

Table 5
Experimental microwave transition frequencies of ^{34}SSO and S^{34}SO (MHz) and residuals (kHz)

Transition	^{34}SSO		S^{34}SO	
	Frequency	*o–c*	Frequency	*o–c*
$2_{1,2}$–$3_{0,3}$	8496.5327(20)	1.3	–	
$1_{0,1}$–$0_{0,0}$	9281.2915(20)	−1.2	9506.9292(20)	0.4
$2_{1,2}$–$1_{1,1}$	18040.8770(20)	−0.4	18451.9443(30)	−0.8
$1_{1,1}$–$2_{0,2}$	18277.3496(20)	−0.4	16594.2647(30)	0.4
$2_{0,2}$–$1_{0,1}$	18557.0381(20)	−0.5	19007.2129(20)	0.3
$2_{1,1}$–$1_{1,0}$	19084.4541(30)	−0.1	19575.9160(20)	−0.4
$3_{1,3}$–$2_{1,2}$	27057.8077(20)	0.2	27673.7266(30)	−0.5
$3_{0,3}$–$2_{0,2}$	27821.6973(20)	1.3	28494.2129(20)	−0.6
$3_{1,2}$–$2_{1,1}$	28623.0997(20)	1.2	29359.5928(30)	−1.5
$4_{1,4}$–$3_{1,3}$	36070.5801(40)	1.7	36890.5469(40)	−1.8
$4_{0,4}$–$3_{0,3}$	37069.7461(20)	0.5	37961.3281(20)	1.5
$1_{1,0}$–$1_{0,1}$	37356.1856(20)	1.0	36163.4707(20)	−0.2
$2_{1,1}$–$2_{0,2}$	37883.5977(20)	−2.5	36732.1739(20)	−0.8
$4_{1,3}$–$3_{1,2}$	38157.3906(30)	−2.5	38774.2950(40)	−2.5
$3_{1,2}$–$3_{0,3}$	38685.0039(30)	1.3	37597.5567(20)	1.2

Table 6
Millimeter wave transition frequencies of ^{34}SSO and S^{34}SO and residuals (MHz)

Transition	Frequency	*o–c*
^{34}SSO		
$10_{1,10}$–$9_{1,9}$	89992.867(20)	−0.018
$10_{6,4}$–$9_{6,3}$	92863.248(30)	−0.024
$10_{6,5}$–$9_{6,4}$	92863.248(30)	−0.024
$10_{7,3}$–$9_{7,2}$	92864.074(30)	0.037
$10_{7,4}$–$9_{7,3}$	92864.074(30)	0.037
$10_{5,6}$–$9_{5,5}$	92868.579(30)	−0.002
$10_{5,5}$–$9_{5,4}$	92868.579(30)	−0.002
$10_{8,2}$–$9_{8,1}$	92868.579(30)	−0.002
$10_{8,3}$–$9_{8,2}$	92868.579(30)	−0.002
$10_{9,1}$–$9_{9,0}$	92875.605(20)	−0.004
$10_{9,2}$–$9_{9,1}$	92875.605(20)	−0.004
$10_{4,7}$–$9_{4,6}$	92886.061(30)	−0.004
$10_{4,6}$–$9_{4,5}$	92886.061(30)	−0.004
$10_{3,8}$–$9_{3,7}$	92921.212(20)	0.010
$10_{3,7}$–$9_{3,6}$	92949.775(20)	−0.020
$17_{2,15}$–$17_{1,16}$	93100.348(20)	0.003
$16_{2,14}$–$16_{1,15}$	93212.153(20)	0.009
$18_{2,16}$–$18_{1,17}$	93399.535(20)	−0.008
$10_{2,8}$–$9_{2,7}$	93553.021(30)	−0.005
$15_{2,13}$–$15_{1,14}$	93692.658(20)	−0.006
$19_{2,17}$–$19_{1,18}$	94148.228(20)	0.006
$14_{2,12}$–$14_{1,13}$	94495.780(20)	−0.001
$7_{1,7}$–$6_{0,6}$	94992.784(20)	−0.003
$10_{1,9}$–$9_{1,8}$	95179.747(20)	−0.002
$20_{2,18}$–$20_{1,19}$	95381.318(40)	0.007
$13_{2,11}$–$13_{1,12}$	95571.798(20)	0.014
$12_{2,10}$–$12_{1,11}$	96867.987(20)	−0.001
$21_{2,19}$–$21_{1,20}$	97130.472(20)	−0.004
$13_{0,13}$–$12_{1,12}$	97920.594(20)	0.013
$11_{2,9}$–$11_{1,10}$	98329.676(20)	−0.013
S^{34}SO		
$16_{2,14}$–$16_{1,15}$	90039.597(20)	0.002
$15_{2,13}$–$15_{1,14}$	90201.093(20)	0.010
$17_{2,15}$–$17_{1,16}$	90316.885(40)	−0.042
$14_{2,12}$–$14_{1,13}$	90752.799(20)	0.009
$18_{2,16}$–$18_{1,17}$	91077.117(20)	–0.002
$1_{20,12}$ − $1_{11,11}$	91425.196(20)	−0.002
$13_{2,11}$–$13_{1,12}$	91641.535(20)	0.000
$10_{1,10}$–$9_{1,9}$	92008.886(20)	0.006
$19_{2,17}$–$19_{1,18}$	92359.944(20)	0.004
$12_{2,10}$–$12_{1,11}$	92809.946(20)	−0.008
$10_{0,10}$–$9_{0,9}$	94008.558(20)	−0.002
$11_{2,9}$–$11_{1,10}$	94197.380(20)	−0.006
$20_{2,18}$–$20_{1,19}$	94201.257(20)	−0.002
$10_{2,9}$–$9_{2,8}$	94897.930(20)	0.000
$10_{7,3}$–$9_{7,2}$	95124.426(40)	0.029
$10_{7,4}$–$9_{7,3}$	95124.426(40)	0.029
$10_{6,4}$–$9_{6,3}$	95125.417(40)	0.019
$10_{6,5}$–$9_{6,4}$	95125.417(40)	0.019
$10_{8,2}$–$9_{8,1}$	95127.550(40)	−0.022
$10_{8,3}$–$9_{8,2}$	95127.550(40)	−0.022
$10_{5,6}$–$9_{5,5}$	95133.457(30)	0.005
$10_{5,5}$–$9_{5,4}$	95133.457(30)	0.005
$10_{9,1}$–$9_{9,0}$	95133.457(30)	0.005
$10_{9,2}$–$9_{9,1}$	95133.457(30)	0.005
$10_{4,7}$–$9_{4,6}$	95155.654(30)	−0.055
$10_{4,6}$–$9_{4,5}$	95155.654(30)	−0.055
$10_{3,8}$–$9_{3,7}$	95197.044(20)	0.016
$10_{3,7}$–$9_{3,6}$	95235.157(30)	−0.014

(*continued on next page*)

Table 6 (*continued*)

Transition	Frequency	*o–c*
$10_{2,8}$–$10_{1,9}$	95741.169(20)	−0.015
$10_{2,8}$–$9_{2,7}$	95950.783(40)	−0.024
$21_{2,19}$–$21_{1,20}$	96633.287(20)	0.001
$9_{2,7}$–$9_{1,8}$	97378.341(20)	0.017
$10_{1,9}$–$9_{1,8}$	97587.953(20)	0.005

Table 7
Rotational constants of ^{34}SSO and S^{34}SO (MHz)

Parameter	^{34}SSO	S^{34}SO
A	41737.0575(23)	40637.0055(25)
B	4901.57321(50)	5034.49061(54)
C	4379.72661(51)	4472.44565(54)
$\Delta_J\times10^3$	1.7815(23)	1.8552(24)
$\Delta_{JK}\times10^3$	−30.795(45)	−29.401(65)
Δ_K	1.1827(20)	1.1224(18)
$\delta_J\times10^3$	0.31585(78)	0.34428(75)
$\delta_K\times10^3$	12.03(20)	12.07(22)
$\Phi_{KJ}\times10^6$	−4.97(56)	−4.35(116)

Higher-order centrifugal distortion constants were constrained to those of the main species (Table 4, Fit 1).

species. The upper spectrum is the result of about 25 min of integration time. In addition to the three hfs components of the $1_{0,1}$–$0_{0,0}$ transition, six hfs components of the $2_{0,2}$–$1_{0,1}$ transition were also measured for both molecules. The experimental transition frequencies are summarized in Table 8, which also gives the transition frequencies of four hfs components of the $6_{1,6}$–$5_{0,5}$ *b*-type transition of ^{33}SSO that were observed at 88 GHz and helped to determine its *A* rotational constants.

Observation of the $1_{0,1}$–$0_{0,0}$ and $2_{0,2}$–$1_{0,1}$ transitions of the prolate asymmetric rotors ^{33}SSO and S^{33}SO with almost all of its hfs components yields $B+C$, χ_{aa}, and $C_{bb}+C_{cc}$. The effects of asymmetry in ^{33}SSO and S^{33}SO are very small in the $2_{0,2}$–$1_{0,1}$ transition, nevertheless they are large enough to allow the determination of χ_{bb} for both isotopic species but its uncertainty is about two orders of magnitude larger than that of χ_{aa}. The effects of centrifugal distortion are small enough and asymmetry is large enough to yield *B* and *C* separately rather than $B+C$ and Δ_J.

The two sets of rotational parameters of ^{33}SSO and S^{33}SO are shown in Table 9. As can be seen the rotational constants from the $r_{I,\varepsilon}$ structure show very good agreement with the experimentally determined values. Comparison of the theoretical and measured nuclear quadrupole coupling constants confirms that the B3LYP/cc-pCVTZ calculation provides a reliable estimate that is accurate to within 10%.

3.4. S_2O_2

The rotational spectrum of S_2O_2 (connectivity: OSSO) was first observed by Lovas et al. [21] in a discharge of SO_2. In analogy to its isovalent pure sulfur analog S_4, the molecule has C_{2v} symmetry with the two SO moieties arranged in a trapezoidal, *cis*-planar configuration. Several transitions of S_2O_2 were observed at centimeter wavelengths in the discharge of SO_2, including six new transitions and four that were remeasured to much higher accuracy than before (Table 10). The derived spectroscopic constants (Table 11) were obtained in two different fits, one based solely on the data in Ref. [21] and the other from a combined fit of the measurements in Table 10 with those in Ref. [21]. Uncertainties in the rotational constants are an order of magnitude smaller and the centrifugal distortion constants are better determined in the combined fit.

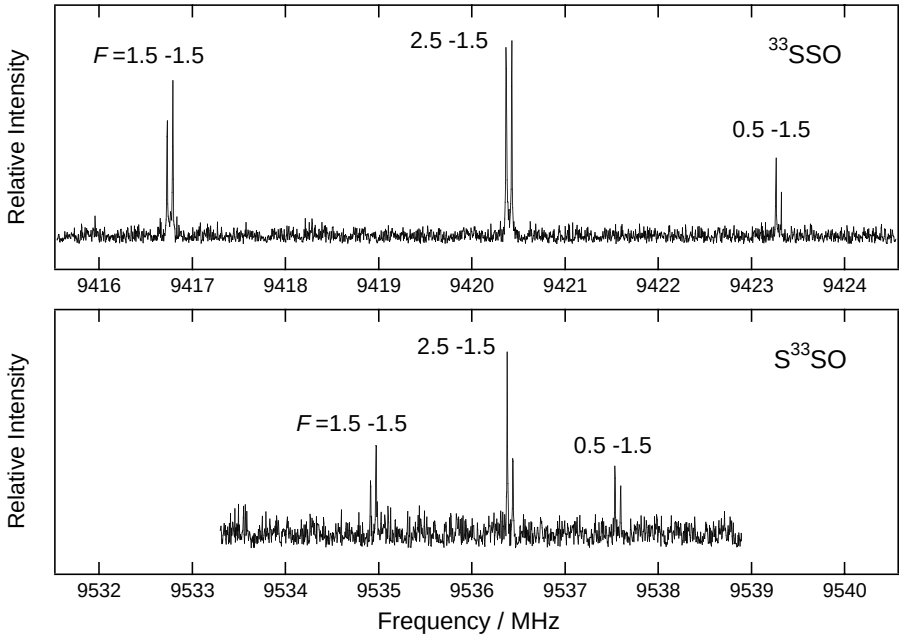

Fig. 3. The $1_{0,1}$–$0_{0,0}$ transitions of ^{33}SSO (upper) and S^{33}SO (lower) exhibiting hyperfine structure from the ^{33}S nucleus. The spectra are composites of single spectra recorded with a step size of 400 kHz. One thousand five hundred cycles were averaged at each setting of the Fabry–Perot cavity employing a repetition rate of 6 Hz.

Table 8
Experimental transition frequencies of ^{33}SSO and S^{33}SO (MHz) and residuals (kHz)

Transition		^{33}SSO		S^{33}SO	
$J'_{K'_a,K'_c} - J''_{K''_a,K''_c}$	$F'–F''$	Frequency	$o–c$	Frequency	$o–c$
$1_{0,1}–0_{0,0}$	1.5–1.5	9416.7601(5)	0.2	9534.9415(5)	0.3
	2.5–1.5	9420.3982(5)	−0.1	9536.4093(5)	−0.4
	0.5–1.5	9423.2923(5)	−0.1	9537.5667(5)	0.1
$2_{0,2}–1_{0,1}$	1.5–0.5	18829.8453(10)	−0.9	19064.3399(10)	−0.8
	2.5–2.5	18830.2219(10)	0.1	19064.5136(10)	−0.4
	0.5–0.5	18833.3759(10)	−0.5	19065.7233(15)	−0.1
	3.5–2.5	18833.7667(5)	0.0	19065.9120(5)	0.2
	2.5–1.5	18833.8607(10)	0.5	19065.9827(5)	0.2
	1.5–1.5	18836.3793(10)	0.6	19066.9656(10)	−0.5
$6_{1,6}–5_{0,5}$	4.5–3.5	88112.555(40)	14.0	–	
	7.5–6.5	88114.215(30)	8.0	–	
	5.5–4.5	88118.942(40)	−47.0	–	
	6.5–5.5	88120.679(50)	28.0	–	

Table 9
Molecular parameters of ^{33}SSO and S^{33}SO (MHz)

Parameter	^{33}SSO		S^{33}SO	
	Prediction[a]	Experiment	Prediction[a]	Experiment
A	41823.2	41823.33(35)	41254.7	41255.7108[b]
B	4978.0	4978.0325(175)	5046.6	5046.6177(154)
C	4441.7	4441.6424(172)	4489.5	4489.5028(151)
$\Delta_J \times 10^3$		1.8365[b]		1.8733[b]
$\Delta_{JK} \times 10^3$		−31.461[b]		−30.764[b]
Δ_K		1.1914[b]		1.1612[b]
$\delta_K \times 10^3$		0.33073[b]		0.34495[b]
$\delta_K \times 10^3$		12.17[b]		12.19[b]
χ_{aa}	−15.6	−14.5260(14)	−5.4	−5.8442(14)
χ_{bb}	33.7	33.90(13)	22.0	22.21(15)
χ_{cc}	−18.1	−19.37(13)[c]	−16.6	−16.37(15)[c]
$(C_{bb}+C_{cc})/2 \times 10^3$		2.84(14)		2.98(14)

[a] Rotational constants from $r_{I,\varepsilon}$ structure, nuclear quadrupole coupling constants from B3LYP/cc-pCVTZ calculation (see Section 3.3).
[b] Constrained (see Section 3.3).
[c] Derived via $\chi_{aa}+\chi_{bb}=-\chi_{cc}$.

4. Discussion

The present study greatly extends the available laboratory rotational data on S_2O. The detection of vibrational satellites from states as high as $\approx 3000\ \mathrm{cm}^{-1}$ (4300 K) above ground emphasizes how well a discharge produces vibrationally hot S_2O, and it is clear that many more vibrational satellites might be detected by the present techniques. Table 12 contains predictions for selected vibrational satellites of S_2O in 12 states not studied here. Detection of these would significantly improve the rotation–vibration parameters of S_2O.

The present FTM work also yields new data on the mono-^{34}S and -^{33}S isotopic species. The nuclear quadrupole coupling constants obtained from quantum chemical calculations at the B3LYP/cc-pCVTZ level of theory are in good agreement with those derived from our measurements. Since the orientation of the electric field gradient principal axes of S^{33}SO differs little from that of $^{33}SO_2$, it is not surprising that the quadrupole constants are also similar, both in sign and magnitude (S^{33}SO vs. $^{33}SO_2$: $\chi_{aa}=-5.8$ vs -1.8 MHz, $\chi_{bb}=$ 22.2 vs. 25.7 MHz, $\chi_{cc}=-16.4$ vs. -23.9 MHz; $^{33}SO_2$ data

Table 10
Experimental microwave transition frequencies of S_2O_2 (MHz) and residuals $o–c$ (kHz)

Transition	Frequency	$o–c$
$2_{1,1}–2_{0,2}$	11013.8404(20)	0.4
$4_{1,3}–4_{0,4}$	14081.6402(20)	0.1
$1_{1,1}–0_{0,0}$	15717.9463(20)	0.6
$4_{0,4}–3_{1,3}$	16714.1670(20)	−1.1
$3_{1,3}–2_{0,2}$	26342.8174(20)	0.0
$4_{2,2}–4_{1,3}$	26553.9151(30)	−3.5
$2_{2,0}–2_{1,1}$	28493.0459(20)	−0.8
$6_{0,6}–5_{1,5}$	30629.2832(30)	−0.6
$5_{2,4}–5_{1,5}$	35295.1993(30)	0.2
$5_{1,5}–4_{0,4}$	35794.5274(20)	1.4

Table 11
Rotational constants of S_2O_2 (MHz)

Parameter	Ref. [21][a]	Present study + Ref. [21]
A	12972.9557 (93)	12972.93037(72)
B	3488.9771 (28)	3488.96986(33)
C	2745.0589 (30)	2745.05543(20)
$\Delta_J \times 10^3$	3.3823(99)	3.3717(44)
$\Delta_{JK} \times 10^3$	−26.770(89)	−26.926(35)
$\Delta_K \times 10^3$	96.863(77)	96.921(38)
$\delta_J \times 10^3$	1.0367(43)	1.0313(17)
$\delta_K \times 10^3$	6.11(12)	6.158(83)
$\Phi_J \times 10^9$	15.7(50)	13.9(24)
$\Phi_{JK} \times 10^6$	0.153(62)	0.087 (30)
$\Phi_{KJ} \times 10^6$	−0.82 (19)	−0.89(15)
$\Phi_K \times 10^6$	3.41 (45)	3.51(43)
$\phi_J \times 10^9$	−8.4(26)	−11.5 (11)
wrms[b]	0.72	0.82

[a] Refitted.
[b] Weighted rms (dimensionless).

Table 12
Frequency predictions for energetically higher vibrational satellites of S_2O not investigated in the present study (MHz)

Transition	(0,9,0)	(0,10,0)	(0,5,1)	(0,6,1)
$1_{0,1}$–$0_{0,0}$	9508.900(2)	9501.612(3)	9493.257(1)	9486.727(2)
$2_{1,2}$–$1_{1,1}$	18404.642(18)	18383.544(28)	18402.361(4)	18382.430(8)
$2_{0,2}$–$1_{0,1}$	19011.178(3)	18996.574(6)	18980.095(2)	18966.991(4)
$2_{1,1}$–$1_{1,0}$	19631.216(22)	19623.175(34)	19570.880(6)	19564.703(11)
Transition	(0,0,2)	(0,1,2)	(0,2,2)	(1,1,0)
$1_{0,1}$–$0_{0,0}$	9479.852(1)	9474.336(1)	9468.623(1)	9539.030(0)
$2_{1,2}$–$1_{1,1}$	18413.250(2)	18395.049(2)	18376.488(2)	18517.789(1)
$2_{0,2}$–$1_{0,1}$	18953.632(1)	18942.535(1)	18931.046(1)	19071.706(1)
$2_{1,1}$–$1_{1,0}$	19506.323(1)	19502.472(2)	19498.190(2)	19638.508(1)
Transition	(1,2,0)	(1,0,1)	(1,1,1)	(2,0,0)
$1_{0,1}$–$0_{0,0}$	9533.204(1)	9501.473(1)	9495.893(1)	9523.095(1)
$2_{1,2}$–$1_{1,1}$	18499.185(1)	18452.327(1)	18434.091(1)	18491.405(2)
$2_{0,2}$–$1_{0,1}$	19059.997(1)	18996.718(1)	18985.495(1)	18985.495(1)
$2_{1,1}$–$1_{1,0}$	19633.818(1)	19553.730(1)	19549.656(1)	19601.137(2)

taken from Ref. [22]).[2] Differences in the electronic environment of the central sulfur atom are evident however in χ_{cc}, since the c inertial axes in S_2O and SO_2 are collinear. Because of the different orientations of the molecules in the ab planes, direct comparison of χ_{aa} and χ_{bb} is of limited value. The off-diagonal coupling constants $|\chi_{ab}|$ were calculated theoretically to be roughly 11 and 7 MHz for ^{33}SSO and S^{33}SO, respectively, but they could not be determined experimentally. Additional rotational data on the ^{33}S isotopic species, especially b-type transitions and a-type transitions with $K_a > 0$, would be of help in determining the A rotational constant of S^{33}SO experimentally.

The two sets of rotational constants of the main isotopic species $^{32}S_2O$ in Table 4 require a brief consideration. For a planar molecule in its equilibrium configuration, the inertial defect $\Delta_e = I_c^e - I_b^e - I_c^e = 0$. The ground state moments of inertia usually yield a small positive value Δ_0, owing to contributions from (i) zero-point vibration, (ii) centrifugal distortion, and (iii) electron–rotation interaction, i.e. $\Delta_0 = \Delta_{vib} + \Delta_{cent} + \Delta_{elec}$ [23]. Lindenmayer et al. [6] derived a value of $\Delta_e = -0.0075$ amu Å^2 for S_2O, but their estimate still contains contributions from higher-order rotation–vibration and electron–rotation interactions. In the present investigation, information about higher-order rotation–vibration interaction has been obtained (Table 4, Fit 2). To evaluate the inertial defect, the rotational equilibrium constants have been corrected for small effects of quartic centrifugal distortion as outlined in Ref. [23]. $\Delta_{cent} = 0.0009$ amu Å^2 has been derived from the quadratic force field (cf. Ref. [24]). Our estimate of $\Delta_{elec} = -0.0052$ amu Å^2 is somewhat larger than $\Delta_{elec} = -0.0037$ amu Å^2 determined for SO_2 [25], but it may still depend on further higher-order vibration–rotation contributions owing to uncertainties in Δ_{vib} and Δ_{cent}. Further refinement in this estimate would require extending the measurements to energetically higher vibrational states and to higher frequencies.

S_2O is a plausible candidate for astronomical detection. Over ten percent of the molecules detected in space so far contain sulfur[3] and the oxides SO and SO_2 are particularly abundant, especially in star-forming regions such as Orion, where line emission from SO_2 is found to contribute substantially to the cooling of the molecular gas [27]. S_2O may also be present in comets, where S, S_2, SO, and SO_2 have already been detected [28]. It is a plausible constituent of planetary atmospheres such as that of Venus [29] or Jupiter's Galilean moon Io where it is thought to be released into the atmosphere by volcanic eruptions or formed by photochemical reactions [30–32]. The laboratory data on S_2O discussed here should allow very sensitive radio astronomical searches for this molecule, both with large single-dish telescopes and with present interferometers. Frequency predictions as well as the global fit file of S_2O can be found online at the CDMS at http://www.cdms.de.

Searches for other exotic sulfur oxides in our molecular beam are worth doing. To date, trisulfur monoxide, S_3O, has only been observed by mass spectrometry [33], which does not yield the molecular structure. Recent ab initio calculations indicate that a branched C_S isomer (S_3 ring with an out-of-plane oxygen atom bound to one of the sulfur atoms) is the global minimum on the potential energy surface [34]. B3LYP/cc-pVTZ calculations for this isomer done in the course of the present study yield $A = 5984.7$ MHz, $B = 3353.0$ MHz, $C = 2401.5$ MHz, $\mu_a = 0.82$ D, and $\mu_c = 1.45$ D. The low-lying c-type rotational transition $1_{1,0}$–$0_{0,0}$ at about 9337.7 MHz ($A + B$) falls in the band where our FTM spectrometer is most sensitive.

[2] It may be noted that a DFT calculation with a smaller basis set (B3LYP/cc-pVTZ) also yields good results: ^{33}SSO: $\chi_{aa} = -15.5$ MHz, $\chi_{bb} = 33.0$ MHz, $\chi_{cc} = -17.5$ MHz; S^{33}SO: $\chi_{aa} = -5.4$ MHz, $\chi_{bb} = 22.0$ MHz, $\chi_{cc} = -16.6$ MHz.

[3] See the Cologne Database for Molecular Spectroscopy, CDMS [26], at http://www.cdms.de, for an up to date list of astronomically detected molecules.

Acknowledgements

This work was supported in part by NASA grant NAG5-9379 and NSF grant CHE-0353693. S. Thorwirth is grateful to the Alexander von Humboldt-Foundation for a Feodor Lynen research fellowship. P. Theulé would like to thank the Swiss National Science Foundation for a research fellowship. H.S.P. Müller acknowledges support by the Deutsche Forschungsgemeinschaft through SFB 494.

References

[1] D.J. Meschi, R.J. Myers, J. Mol. Spectrosc. 3 (1959) 405–416.
[2] R.L. Cook, G. Winnewisser, D.C. Lindsey, J. Mol. Spectrosc. 46 (1973) 276–284.
[3] E. Tiemann, J. Hoeft, F.J. Lovas, D.R. Johnson, J. Chem. Phys. 60 (1974) 5000–5004.
[4] J. Lindenmayer, J. Mol. Spectrosc. 116 (1986) 315–319.
[5] J. Lindenmayer, H. Jones, J. Mol. Spectrosc. 112 (1985) 71–78.
[6] J. Lindenmayer, H.D. Rudolph, H. Jones, J. Mol. Spectrosc. 119 (1986) 56–67.
[7] T. Müller, P.H. Vaccaro, F. Pérez-Bernal, F. Iachello, J. Chem. Phys. 111 (1999) 5038–5055.
[8] R. Steudel, Top. Curr. Chem. 231 (2003) 203–230.
[9] M.C. McCarthy, S. Thorwirth, C.A. Gottlieb, P. Thaddeus, J. Am. Chem. Soc. 126 (2004) 4096–4097.
[10] M.C. McCarthy, S. Thorwirth, C.A. Gottlieb, P. Thaddeus, J. Chem. Phys. 121 (2004) 632–635.
[11] S. Thorwirth, M.C. McCarthy, C.A. Gottlieb, P. Thaddeus, H. Gupta, J.F. Stanton, J. Chem. Phys. 123 (2005) 054326.
[12] M.C. McCarthy, M.J. Travers, A. Kovacs, C.A. Gottlieb, P. Thaddeus, Astrophys. J. Suppl. Ser. 113 (1997) 105–120.
[13] M.C. McCarthy, W. Chen, M.J. Travers, P. Thaddeus, Astrophys. J. Suppl. Ser. 129 (2000) 611–623.
[14] M.E. Sanz, M.C. McCarthy, P. Thaddeus, J. Chem. Phys. 122 (2005) 194319.
[15] C.A. Gottlieb, P.C. Myers, P. Thaddeus, Astrophys. J. 588 (2003) 655–661.
[16] H.M. Pickett, J. Mol. Spectrosc. 148 (1991) 371–377.
[17] G. Herzberg, Molecular Spectra and Molecular Structure, 2, Krieger Publishing Co., Malabar, Florida, 1991.
[18] H.D. Rudolph, Struct. Chem. 2 (1991) 581–588.
[19] H.S.P. Müller, M.C.L. Gerry, J. Chem. Soc. Faraday Trans. 90 (1994) 2601–2610.
[20] M.J. Frisch, G.W. Trucks, H.B. Schlegel, et al., GAUSSIAN 03, Revision B.04, Gaussian, Inc., Wallingford, CT 2003
[21] F.J. Lovas, E. Tiemann, D.R. Johnson, J. Chem. Phys. 60 (1974) 5005–5010.
[22] H.S.P. Müller, J. Farhoomand, E.A. Cohen, B. Brupbacher-Gatehouse, M. Schäfer, A. Bauder, G. Winnewisser, J. Mol. Spectrosc. 201 (2000) 1–8.
[23] W. Gordy, R.L. Cook, Microwave Molecular Spectra, third ed., Wiley, New York, 1984.
[24] D. Christen, J. Mol. Struct. 48 (1978) 101–106.
[25] T. Oka, Y. Morino, J. Mol. Spectrosc. 8 (1962) 9–21.
[26] H.S.P. Müller, S. Thorwirth, D.A. Roth, G. Winnewisser, Astron. Astrophys. 370 (2001) L49–L52.
[27] C. Comito, P. Schilke, T.G. Phillips, D.C. Lis, F. Motte, D. Mehringer, Astrophys. J. Suppl. Ser. 156 (2005) 127–167.
[28] D. Bockelée-Morvan, J. Crovisier, ESA SP-460: The Promise of the Herschel Space Observatory, 2001, pp. 279–286.
[29] C.Y. Na, L.W. Esposito, Icarus 125 (1997) 364–368.
[30] M.Y. Zolotov, B. Fegley, Icarus 133 (1998) 293–297.
[31] J.I. Moses, M.Y. Zolotov, B. Fegley, Icarus 156 (2002) 76–106.
[32] R. Steudel, Y. Steudel, Eur. J. Inorg. Chem. (2004) 3513–3521.
[33] F. Cacace, G. de Petris, M. Rosi, A. Troiani, Chem. Commun. (2001) 2086–2087.
[34] M.W. Wong, R. Steudel, Chem. Commun. (2005) 3712–3714.